



Flow drill riveting of carbon fiber-reinforced polymer and aluminum alloy sheets

Shuang Wang¹ · Junying Min¹ · Jianping Lin¹ · Hailang Wan¹ · Yunqing Wang²

Received: 23 January 2019 / Accepted: 23 March 2019 / Published online: 10 April 2019
© International Institute of Welding 2019

Abstract

As a variation of friction stir blind riveting, flow drill riveting (FDR) is a new one-sided mechanical joining method for similar and/or dissimilar materials without predrilling holes on workpieces. In the FDR process, a blind rivet with a conical mandrel tip rotates at a high spindle speed and penetrates the workpieces due to local softening as a result of high friction between the mandrel tip and workpieces. The FDR process was applied to fabricating dissimilar lap-shear joints of 2.0-mm-thick carbon fiber-reinforced polymer (CFRP) and aluminum alloys (AA6061) with thicknesses of 1.0, 1.5, and 2.0 mm in this work. The effects of the thickness of AA6061 and stack-up sequence of CFRP and AA6061 on the maximum tensile load and failure mode of FDR joints were analyzed and discussed. With the increase of AA6061 thickness, the maximum tensile load increased and the failure mode changed from failure at the AA6061 to failure at the CFRP disregarding their stack-up sequence. It is found that the maximum tensile load and the failure mode are strongly dependent on the relatively weaker one of AA6061 and CFRP workpieces, and the maximum tensile load of the FDR joint is closely related to its failure mode.

Keywords Dissimilar material joining · Composite · Al alloy · Friction stir

1 Introduction

Carbon fiber-reinforced polymer (CFRP) and aluminum alloy owing to the low densities and high mechanical performance are two important lightweight materials and have been increasingly applied in automobile field [1–3]. However, conventional joining methods (e.g., resistance spot welding (RSW)) are not capable of joining metals and CFRP due to incompatible thermophysical properties [4, 5]. In order to solve the joining issue of dissimilar materials, riveting technologies (e.g., self-pierce riveting (SPR) [6], clinching [7], spin blind riveting (SBR) [8], friction stir blind riveting

(FSBR) [9]), and flow drill screw (FDS) [10] have been developed.

SPR and clinching have been widely used as joining technologies in the automobile manufacturing field due to relatively high fatigue strength compared with RSW [11–13]. The fatigue strength of SPR joints from the AA5182 was about twice higher than that of RSW joints when the fatigue lives ranged from 10^5 to 10^6 cycles [14]. Krause et al. [15] found that both SPR and clinching joints had superior fatigue strength at 10^6 cycles than RSW joints from the AA5754. However, both clinching and SPR belong to two-sided joining technology, i.e., dies need to be placed on both sides of the joints to complete the joining processes, which restricts their applications in closed or semi-closed structures [16]. In such a situation, the single-sided joining technology of FDS has been developed in vehicle manufacturing industries, which is achieved by the high-speed rotating screw penetrating through both workpieces and thread engagement forming [17, 18]. Afterwards, Nagel et al. [19] proposed an optimized screw for joining CFRP and AW6181 to achieve a better thread profile and push-out strength. Besides, SBR was developed to join glass fiber-reinforced polyamide and metal such as magnesium or aluminum alloys, which was implemented by a blind rivet with a spindle speed of 2000 rpm or even more

Recommended for publication by Commission III - Resistance Welding, Solid State Welding, and Allied Joining Process

✉ Junying Min
Junying.Min@tongji.edu.cn

✉ Jianping Lin
jplin58@tongji.edu.cn

¹ School of Mechanical Engineering, Tongji University, Shanghai 201804, China

² EPRESS Systems (Shenzhen) Ltd, Shenzhen 51809, China

pressing into the workpieces and locking them by expanded shank tail, as shown in Fig. 1 [8]. Podlesak et al. [8] found that the tensile load of SBR joints increased maximum by 68%, compared with that of conventional riveting joints. FSBR invented by Wang et al. [20] was also a single-sided joining technology, which used a blind rivet rotating at a high spindle speed to penetrate through the workpieces and lock them by expanded shank tail, as shown in Fig. 1. The FSBR was used by Min et al. [21] to join CFRP and AA6111, and it is found that the material stack-up sequence had an effect on the maximum tensile load and failure mode. In addition, the effect of material matching on the maximum tensile load was also studied, and the results showed that the maximum tensile load of the joints depended on relatively weaker materials [22]. Besides, a modified blind rivet with sharp mandrel tip was also applied in FSBR to reduce the penetration force [16].

A new single-sided mechanical joining method of flow drill riveting (FDR) has been proposed to join similar and/or dissimilar materials in the present study, which not only combines the advantages of SBR and FSBR but also has a unique locking mechanism resulting from the newly designed blind rivet. In the FDR process, as illustrated in Fig. 1, a blind rivet with a conical mandrel tip rotates at a high spindle speed and

penetrates through the workpieces. The frictional heat is generated between the mandrel tip of the blind rivet and workpieces, where local material is heated and then softened resulting in reducing the penetration force. When the shank head of blind rivet touches the upper workpiece (i.e., the penetration stroke of the blind rivet reaches 18.5 mm), the rivet stops penetrating and rotating. Then, the mandrel body is pulled and broken at its pre-set notch compressing the shank tail to its buckling limit, which results in the formation of a folded shank between the mandrel tip and lower workpiece as shown in Fig. 1. Finally, the workpieces are locked tightly by the shank fold and shank head of the blind rivet, which is a special locking mechanism other than those of SBR and FSBR.

In this study, FDR joints were successfully fabricated from 2.0-mm-thick CFRP and AA6061 with thicknesses of 1.0, 1.5, and 2.0 mm, including six groups in terms of two stack-up sequences and three thicknesses of AA6061 workpieces. The quasi-static single lap-shear tensile testing was carried out to test mechanical properties of FDR joints. The effects of stack-up sequence and AA6061 thickness on the maximum tensile load and failure mode of FDR joints were analyzed and discussed.

Blind riveting method	Process				Cross-sections of rivets	Shank deformation	Locking mechanisms
	(a)	(b)	(c)	(d)			
Spin Blind Riveting (SBR)					 4.8mm	Expanding	
Friction Stir Blind Riveting (FSBR)					 6.4mm	Expanding	
Flow Drill Riveting (FDR)					 6.4mm	Folding	

Fig. 1 Process, type of rivet, cross-sections of rivets, shank deformation, and locking mechanisms of the SBR, FSBR, and FDR. **a** The blind rivet approaches and penetrates the workpieces with a feed rate of f and a

spindle speed of ω . **b** The rivet stops penetrating and rotating as the shank head touches the upper workpiece. **c** The mandrel body is pulled with a force of F . **d** The mandrel body is broken at its pre-set notch [8, 21]

Table 1 Specific parameters of SYT45-T700 carbon fibers

Tow	Elongation (%)	Density (g/cm ³)	Per fiber diameter (um)
12 K	1.9	1.79	7

2 Experimental details

2.1 Materials

The 2.0-mm-thick CFRP sheets and hot rolled AA6061 sheets with thicknesses of 1.0, 1.5, and 2.0 mm were chosen as experimental materials in this work. The CFRP sheets were consisted of SYT45-T700 carbon fibers and thermoset epoxy resin. The specific parameters of SYT45-T700 carbon fibers are listed in Table 1. The CFRP sheets were anisotropic and included 11 prepreg plies laid up in 0°/90° bidirectional configuration. The mechanical properties of CFRP and AA6061 sheets were obtained from uniaxial tensile tests and listed in Table 2, where the length direction of tested CFRP uniaxial tensile specimens was consistent with the ply direction of its top layer prepreg. CFRP and AA6061 sheets were cut into workpieces having a size of 127 × 38 mm² to fabricate FDR joints, and the length direction of workpieces was aligned with the rolling direction of AA6061 and the ply direction of the top layer prepreg of CFRP. The blind rivet used in FDR process was a newly designed blind rivet with a conical mandrel tip (i.e., about 77°) to improve the local softening and reduce the penetration force, as illustrated in Fig. 1. The dimensions of the specially designed blind rivet are presented in Fig. 2, where the shank and mandrel of the rivet were made from mild steel and #45 steel, respectively.

Table 2 Mechanical properties of the CFRP and AA6061 sheets at room temperature

Materials	Young's modulus (GPa)	Tensile strength (MPa)	Yield strength (MPa)	Fracture elongation (%)
CFRP	74	926	–	1.4
AA6061	68	290	255	28

2.2 Fabrication of FDR joints

There are six groups of lap-shear joints by the FDR process considering two stack-up sequences and three thicknesses of AA6061 workpieces, and the FDR joints are designated as AA6061(x)/CFRP or CFRP/AA6061(x) when the AA6061 with a thickness of x mm is placed as the upper and lower workpiece, respectively, as listed in Table 3. The experimental fixture used for clamping workpieces during the fabrication of the FDR joints is shown in Fig. 3, which was fixed on a platform of the NC milling machine (MAG NBF540). The spacers were used to keep the surfaces of to-be-joined workpieces perpendicular to the spindle of the NC milling machine. The overlap region of the workpieces was square with dimensions of 38 × 38 mm². The mandrel body of blind rivet was gripped by the spindle of the NC milling machine. A feed rate of 60 mm min⁻¹ and a spindle speed of 6000 rpm were applied in the FDR process. The penetrating and rotating of the blind rivet stopped as the shank head touched the upper workpiece, and then the mandrel body was pulled to break at its notch with a riveting gun in order to finish the FDR process. The shank tail buckled and ballooned to form a fold below the lower workpiece to lock the penetrated workpieces firmly as shown in Fig. 1d. Figure 4 presents the configurations and detailed dimensions of a single lap-shear FDR joint following [21, 23].

2.3 Quasi-static single lap-shear tensile testing

Quasi-static lap-shear tensile testing of the FDR joints was performed on a MTS universal testing machine. The testing

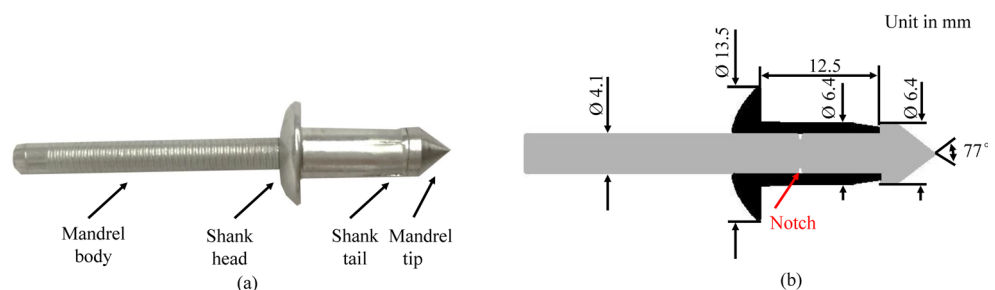
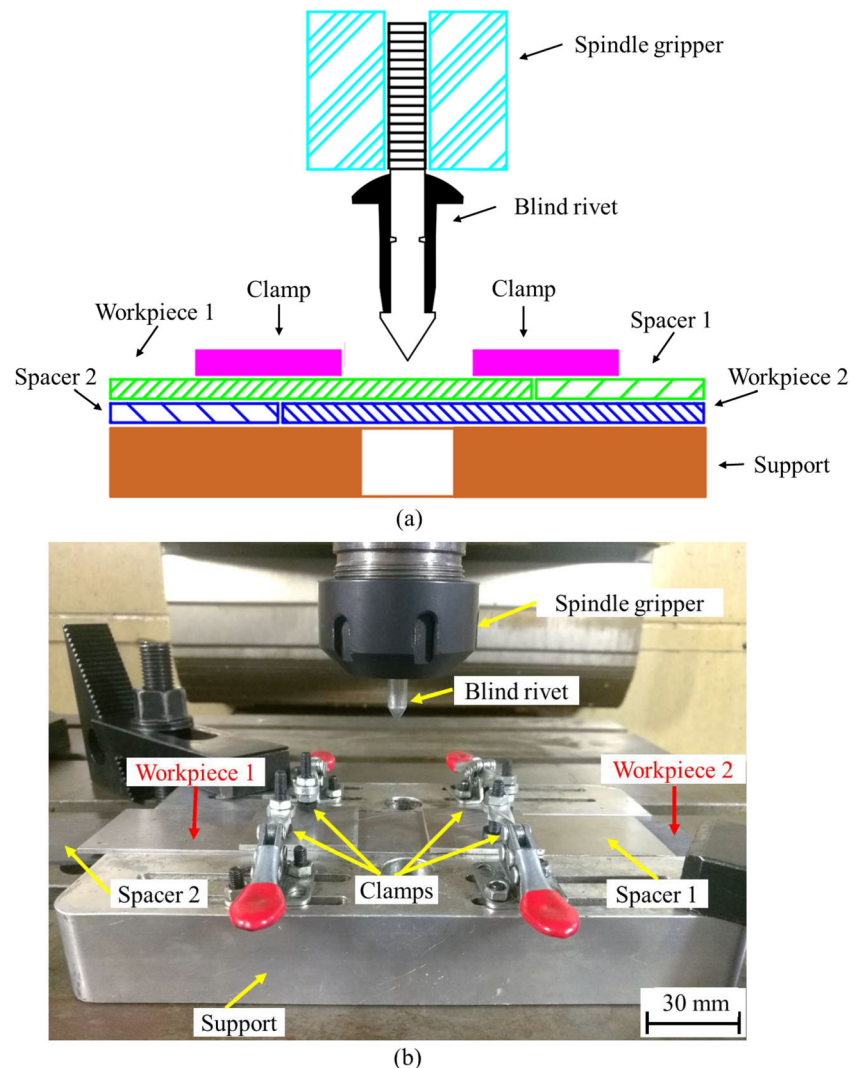
Fig. 2 **a** A photo of the specially designed blind rivet used in FDR process. **b** The dimensions of the blind rivet

Table 3 Combinations of workpiece materials in FDR joints

Material stack-ups	Upper workpiece (thickness)	Lower workpiece (thickness)
AA6061/CFRP	AA6061 (1.0/1.5/2.0)	CFRP (2.0)
CFRP/AA6061	CFRP (2.0)	AA6061 (1.0/1.5/2.0)

process was recorded with a digital camera from the side view of FDR joints to observe their fracture processes. Two filler plates with dimensions of 38 mm × 38 mm were attached to both ends of each joint to accommodate its offset. Then, the FDR joints were loaded to failure at a crosshead speed of 10 mm/min. Three replicates were tested for each material combination and the average maximum tensile load was used to evaluate the mechanical property of the FDR joints. After lap-shear testing, the failure modes of joints were reported and evaluated for the further analyses.

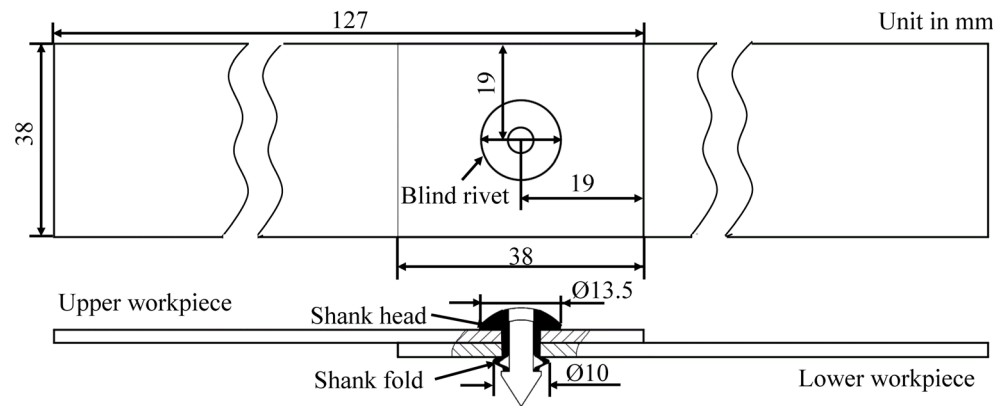
Fig. 3 **a** An illustration and **b** A photo of the experimental fixture used in the FDR process



3 Results and discussion

Figure 5a, b presents semi-finished joints with different stack-up sequences, e.g., AA6061(1.0)/CFRP and CFRP/AA6061(1.0) joints, prior to pulling the rivet mandrels. It is observed that the rivet shank was wrapped by the broken fibers on the AA6061(1.0)/CFRP joint and by the Al material flash on the CFRP/AA6061(1.0) joint. The broken fibers and the Al material flash were formed due to rivet penetration. The FDR joints were successfully finished by pulling rivet mandrels and are shown in Fig. 5c, d. Detailed observations on the

Fig. 4 Configurations and detailed dimensions of a single lap-shear FDR joint



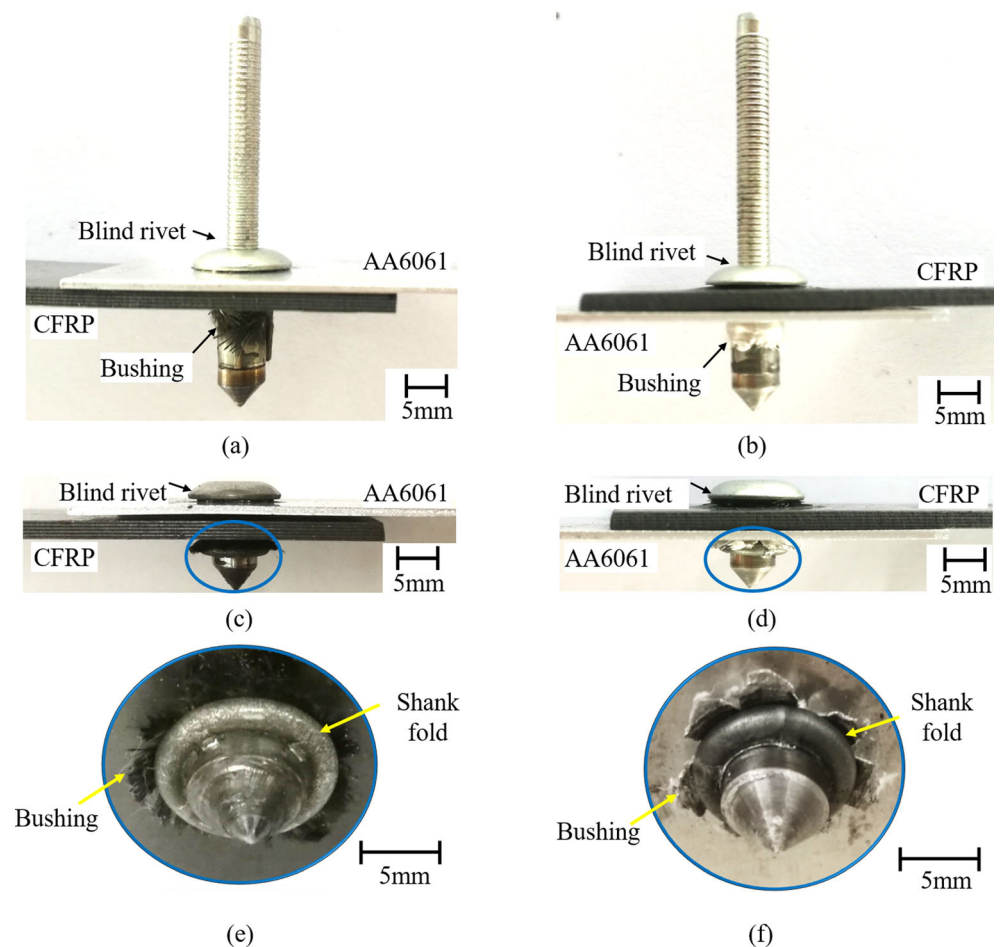
folds of rivet shank on the finished FDR joints are presented in Fig. 5e, f, where the broken fibers or the Al material flash were expanded due to the formation of shank folds. This observation is common disregard of the thicknesses of AA6061.

3.1 Mechanical testing results of FDR joints

The load-displacement curves of each CFRP/AA6061 joint and AA6061/CFRP joint of the repeated three are shown in

Fig. 6a, b, respectively. The CFRP/AA6061 joints generally exhibited larger maximum displacements and the displacements (as denoted by arrows in Fig. 6a, b) corresponding to the maximum loads than AA6061/CFRP joints, except the joints with AA6061(1.0), and the maximum tensile loads and displacements of CFRP/AA6061(1.0) and AA6061(1.0)/CFRP joints are similar as observed from Fig. 6a, b. It can be also found that the displacement of AA6061(1.0)/CFRP joint was larger than that of AA6061(1.5)/CFRP and AA6061(2.0)/

Fig. 5 Photographs of semi-finished **a** AA6061(1.0)/CFRP joint and **b** CFRP/AA6061(1.0) joint, finished **c** AA6061(1.0)/CFRP joint and **d** CFRP/AA6061(1.0) joint, and **e** magnified structure of **c** and **f** magnified structure of **d**



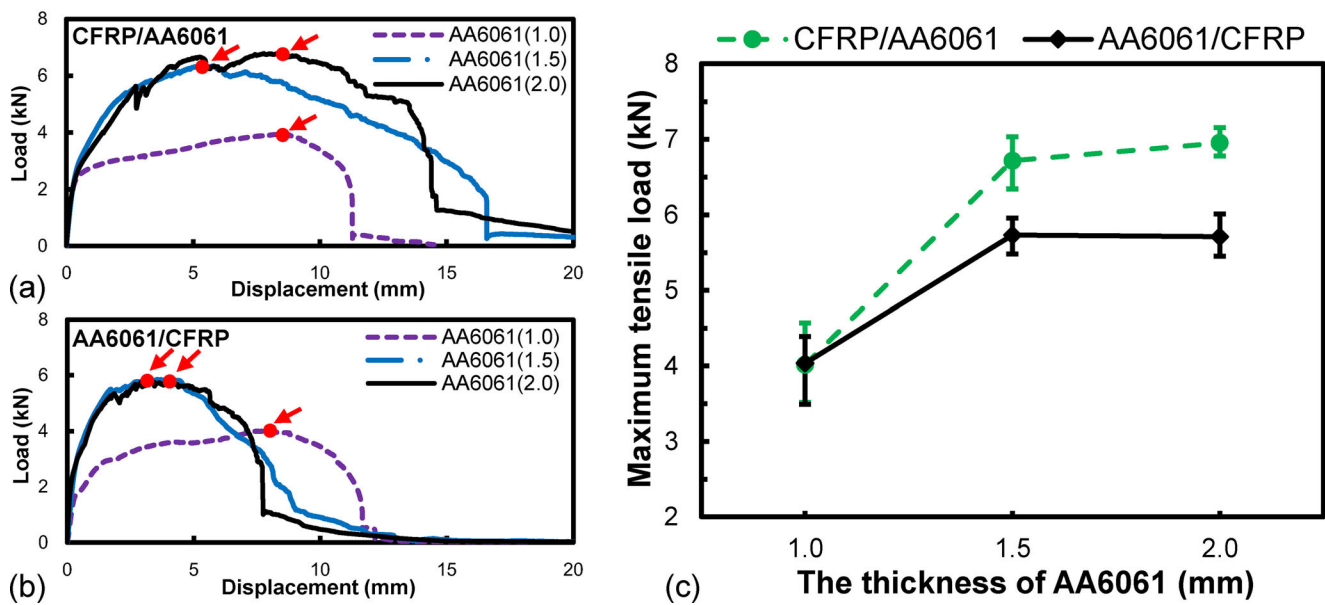


Fig. 6 Load-displacement curves of **a** CFRP/AA6061 and **b** AA6061/CFRP joints and **c** The maximum tensile loads of FDR joints

CFRP joints at their maximum tensile loads in Fig. 6b. However, the tendency was not obvious for CFRP/AA6061 joints. The maximum tensile loads of the FDR joints are summarized in Fig. 6c. As the thickness of AA6061 increased from 1.0 to 1.5 mm, improvements of 42.5% and 67.5% were observed for AA6061(1.5)/CFRP and CFRP/AA6061(1.5) joints when compared with the joints with AA6061(1.0), respectively. The continuous increase of AA6061 thickness exhibits no further improvement on the maximum tensile load of the FDR joints.

The failure modes of AA6061/CFRP joints fabricated by FDR are shown in Fig. 7. The failure position of AA6061(1.0)/CFRP joint was located in AA6061(1.0). The failure mode was that AA6061 was torn out by the blind rivet.

When the thickness of upper AA6061 increased to 1.5 mm, the failure position of AA6061(1.5)/CFRP joint was transferred from upper AA6061 to lower CFRP. The shank fold slipped out from the rivet hole on the lower CFRP, which resulted in hole expansion and delamination of some carbon fibers on the CFRP. Furthermore, the bending of the upper AA6061(2.0) was obviously observed. The AA6061(2.0)/CFRP joint showed the same failure mode with the AA6061(1.5)/CFRP joint, which is consistent with the similar maximum tensile loads of both joints, as shown in Fig. 6.

Figure 8 presents the failure modes of CFRP/AA6061 joints fabricated by FDR. The CFRP/AA6061(1.0) joint failed as the lower AA6061 was torn out, which was similar to failure

Fig. 7 Fractured FDR joints after lap-shear tensile testing. **a** AA6061(1.0)/CFRP. **b** AA6061(1.5)/CFRP. **c** AA6061(2.0)/CFRP

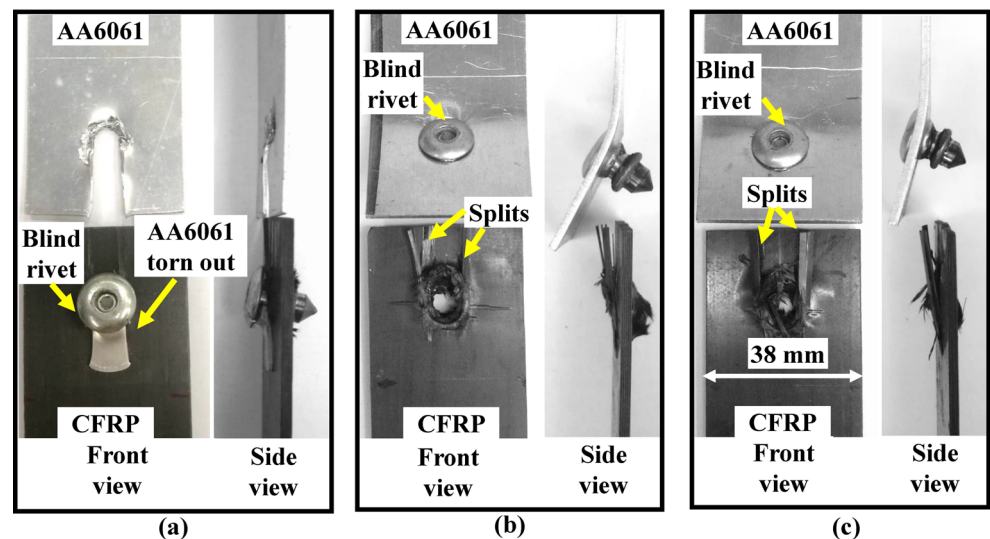
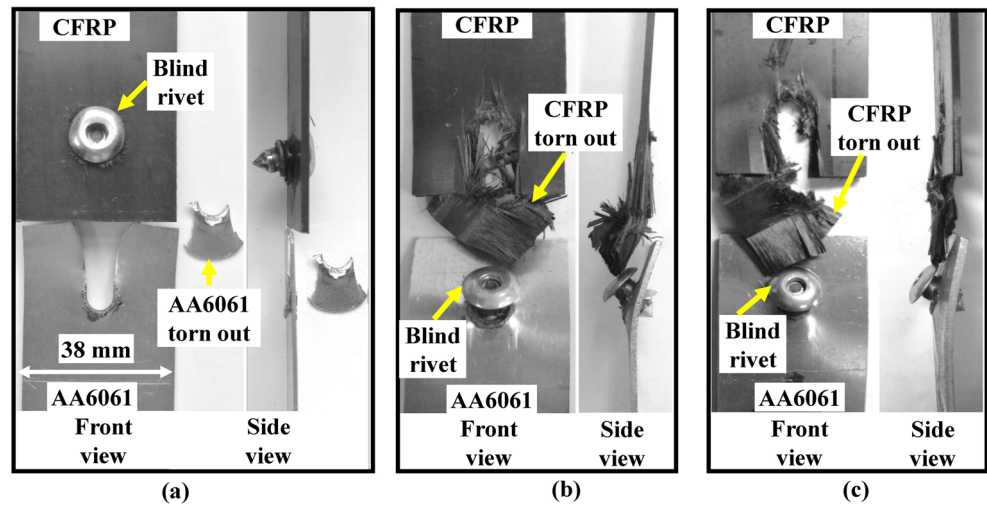


Fig. 8 Fractured FDR joints after lap-shear tensile testing. **a** CFRP/AA6061(1.0), **b** CFRP/AA6061(1.5), **c** CFRP/AA6061(2.0)



mode of AA6061(1.0)/CFRP joint. CFRP/AA6061(1.5) and CFRP/AA6061(2.0) joints had the same failure mode, which was that lower CFRP was torn out by the blind rivet along tensile direction. The same failure mode offered a reasonable explanation for the approximately same maximum tensile loads of CFRP/AA6061(1.5) and CFRP/AA6061(2.0) joints, as shown in Fig. 6. The failure modes of all FDR joints are summarized in Table 4. It is worth noting that failure mode was influenced by not only the thicknesses of AA6061 but also the stack-up sequence of AA6061 and CFRP.

Figure 6 and Table 4 indicate that the FDR joints with 1.5- and 2.0-mm-thick AA6061 have similar maximum tensile loads and failure modes for the given stack-up sequence. Therefore, the FDR joints with AA6061(2.0) were discussed exemplarily in the following subsections. In order to understand the effects of stack-up sequence and AA6061 thicknesses on the maximum tensile loads and failure modes of FDR joints from AA6061 and CFRP, the fracture processes of FDR joints with 1.0- and 2.0-mm-thick AA6061 were further investigated.

The lap-shear testing results are further discussed in terms of material stack-up sequences and the thicknesses of AA6061.

3.2 AA6061/CFRP joints

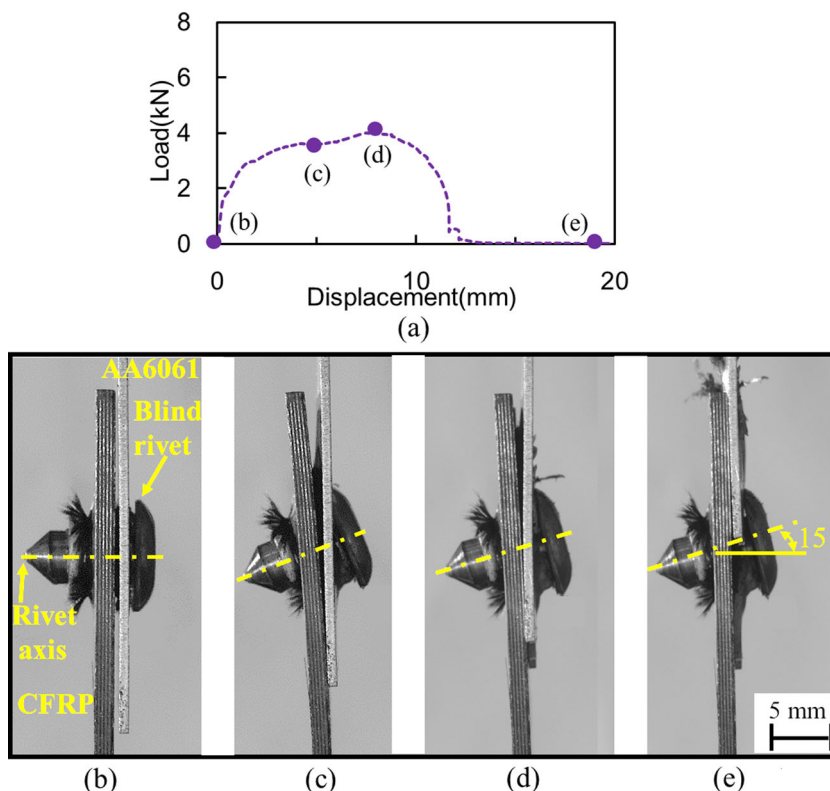
The fracture processes of AA6061(1.0)/CFRP and AA6061(2.0)/CFRP joints in lap-shear tensile testing were discussed in detail to understand the phenomenon that the thickness of AA6061 exhibited an effect on failure modes and the maximum tensile loads of the joints. Figure 9b–c exhibit the a sequence of four images from the side view of AA6061(1.0)/CFRP joint, which were recorded by a digital camera, at four different moments shown in Fig. 9a during lap-shear tensile testing. The blind rivet axis was horizontal and perpendicular to the direction of tensile load before the lap-shear tensile testing, as shown in Fig. 9b. The blind rivet was inclined to ~15° by the torque resulting from the non-collineation of tensile load on AA6061(1.0) and CFRP at the initial stage of the testing in Fig. 9c. However, the continuously increasing load exhibited little benefit to the inclination angle of the blind rivet, as shown in Fig. 9d, e. The AA6061 material close to rivet hole was compressed by the inclined blind rivet during lap-shear tensile testing. When the tensile load exceeded the shear capability of AA6061(1.0), the AA6061(1.0) was torn out by the blind rivet. Nevertheless, the CFRP of this AA6061(1.0)/CFRP joint was nearly un-

Table 4 A summary of the failure mode descriptions of FDR joints

The thickness of AA6061 workpiece (mm)	Failure descriptions			
	AA6061/CFRP joints		CFRP/AA6061 joints	
	AA6061	CFRP	AA6061	CFRP
1.0	Torn out ^a	Unbended	Torn out ^a	Unbended
1.5	Bended	Slipped out by shank fold ^a	Bended	Torn out ^a
2.0	Bended	Slipped out by shank fold ^a	Bended	Torn out ^a

^a Failure workpiece of each FDR joint in lap-shear tensile testing

Fig. 9 Fracture process of AA6061(1.0)/CFRP joint. **a** A typical load-displacement curve. **b–e** Deformation modes at different moments, and the corresponding displacements of the joint are marked in **a**



damaged and unbended due to its much higher shear strength compared to AA6061(1.0). As a result, the upper AA6061(1.0) was torn out and the blind rivet remained on the lower CFRP, as shown in Fig. 7a.

Figure 10b–e shows the fracture process of AA6061(2.0)/CFRP joint during lap-shear tensile testing. When the tensile load was applied to AA6061(2.0)/CFRP joint, the blind rivet started to incline and resulted in the stress concentration at contact point between the upper AA6061(2.0) and the shank head of blind rivet, which caused the bending of AA6061(2.0). The inclination angle of blind rivet and the bending degree of AA6061(2.0) increased gradually with the increase of tensile load, which aggravated the situation that the shank fold of blind rivet fell into the rivet hole on the lower CFRP, as shown in Fig. 10d. At the same time, the rivet hole on the lower CFRP was expanded by the shank fold resulting from the blind rivet inclination. When the blind rivet inclined to a certain angle ($\sim 40^\circ$), the shank fold was slipped out from the expanded rivet hole, as shown in Fig. 10e. It was also found that some carbon fibers were delaminated from the CFRP in Fig. 10e.

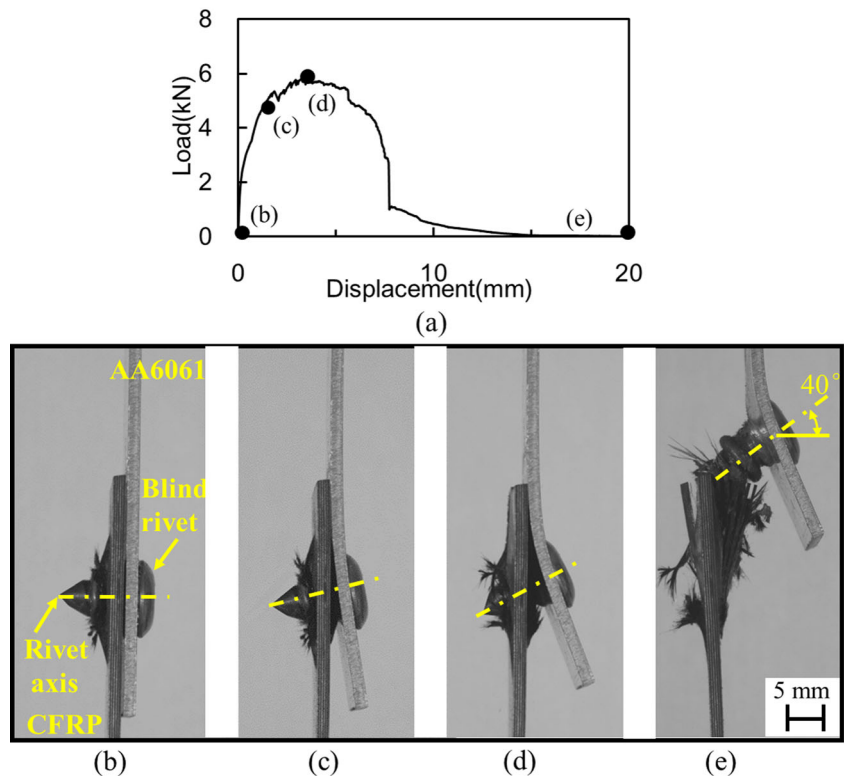
By comparing Figs. 9 with 10, it can be found that there were apparent differences not only in the inclination angle of the blind rivet but also the joint failure position. The blind rivet of AA6061(1.0)/CFRP joint inclined to $\sim 15^\circ$ and then maintained at that level even as the lower AA6061(1.0) was torn out in Fig. 9. Nevertheless, the inclination angle of the blind rivet in the AA6061(2.0)/CFRP joint increased

gradually to $\sim 40^\circ$ in the course of lap-shear tensile testing as shown in Fig. 10e, which is larger than that of AA6061(1.0)/CFRP joint (i.e. $\sim 15^\circ$). Furthermore, a larger inclination angle of blind rivet indicates a more severely expanded rivet hole on CFRP. Therefore, the blind rivet inclining at a larger angle was easier to slip out from the expanded rivet hole on the CFRP. Moreover, the failure mode of AA6061(1.0)/CFRP joint (i.e., the upper AA6061(1.0) was torn out) shows that the maximum tensile load of the joint depends on the mechanical property of AA6061(1.0), which is a weaker one relative to the CFRP. As the thickness of AA6061 increased to 2.0 mm, the weaker workpiece transferred to CFRP, which is indicated by the failure mode of AA6061(2.0)/CFRP joint. The change of failure mode provides an explanation for that the thicker AA6061 (≥ 1.5) resulted in a larger maximum tensile load, and also indicates that the force associated with tearing out the AA6061(1.0) was lower than that required by the shank fold slipping out from the rivet hole on the CFRP.

3.3 CFRP/AA6061 joints

In order to find out the explanation for the effect of the thicknesses of AA6061 workpiece on the failure modes and maximum tensile loads of CFRP/AA6061(1.0) and CFRP/AA6061(2.0) joints, the fracture processes were also investigated in detail in this section. Figure 11b–e presents the fracture process of CFRP/AA6061(1.0) joint. Similarly, a slight inclination of the blind rivet was observed when a

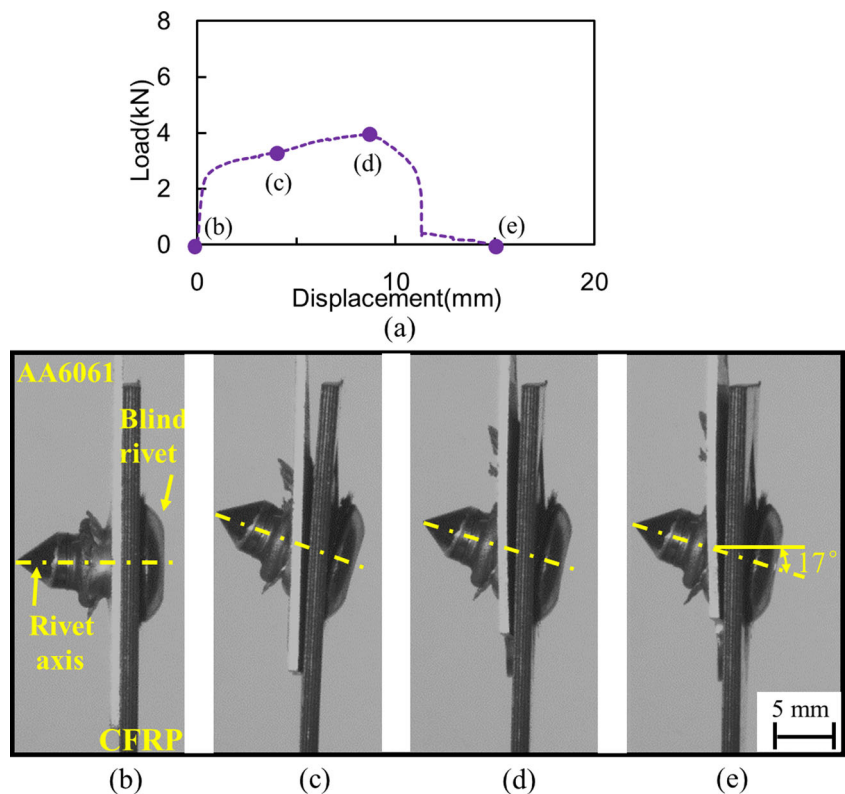
Fig. 10 Fracture process of AA6061(2.0)/CFRP joint. **a** A typical load-displacement curve. **b–e** Deformation modes at different moments, and the corresponding displacements of the joint are marked in **a**



tensile load was applied to the lap-shear joint; however, the inclination angle nearly did not change (i.e., $\sim 17^\circ$) with the development of lap-shear tensile testing. Then,

the AA6061(1.0) was gradually torn out by the inclined blind rivet in CFRP/AA6061(1.0) joint. Nonetheless, it is worth noting that the CFRP of the joint was not

Fig. 11 Fracture process of CFRP/AA6061(1.0) joint. **a** A typical load-displacement curve. **b–e** Deformation modes at different moments, and the corresponding displacements of the joint are marked in **a**



damaged and bended obviously during the lap-shear tensile testing.

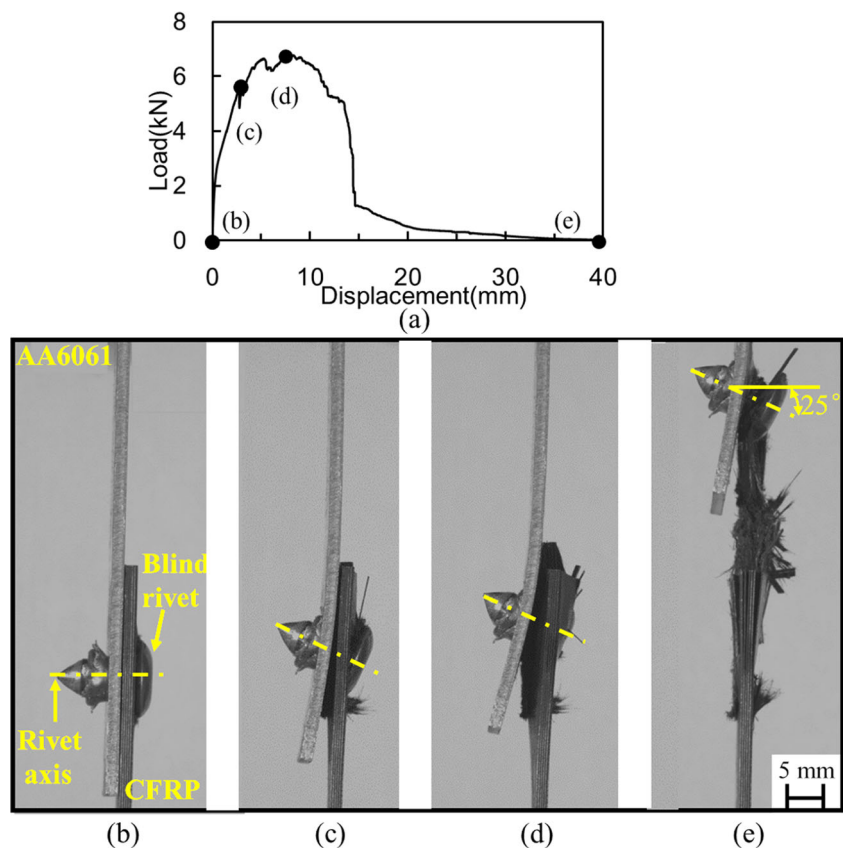
Figure 12b–e shows the fracture process of CFRP/AA6061(2.0) joint. The blind rivet of CFRP/AA6061(2.0) joint started to incline with the lap-shear tensile load being applied. The inclination of blind rivet resulted in local contact between the shank fold and the lower AA6061(2.0), which consequently caused a stress concentration on the AA6061(2.0). Subsequently, the AA6061(2.0) was bended, as shown in Fig. 12c. However, the inclination angle of blind (i.e., $\sim 25^\circ$) rivet and the bending degree of AA6061 showed no more increase with the increasing of tensile load in the later part of lap-shear testing. Finally, the CFRP was torn out as presented in Fig. 12e.

It can be found that the failure position of CFRP/AA6061 joints was transferred from AA6061(1.0) to CFRP, when the thickness of AA6061 workpiece increased from 1.0 to 2.0 mm. As for CFRP/AA6061(1.0) joint, the AA6061(1.0) was torn out by the blind rivet in lap-shear tensile testing. Nevertheless, no obvious damage was observed on the CFRP even when the maximum tensile load of the joint was reached. Therefore, it can be concluded that in the lap-shear tensile testing of CFRP/AA6061 joints, AA6061(1.0) was the weaker one compared to the CFRP. Increasing the thickness of AA6061 from 1.0 to 2.0 mm strengthened the Al alloy side,

and the CFRP became a relatively weaker one compared with AA6061(2.0), which was indicated by the failure mode on the CFRP/AA6061(2.0) joint, where the CFRP was torn out in lap-shear tensile testing. The above suggests that both the failure mode and the maximum tensile load of the FDR joints depend on the tearing resistance of the relatively weaker workpiece. From the maximum tensile loads in Fig. 6c, it can be inferred that the tearing resistance of the CFRP was ~ 3.0 kN higher than that of the AA6061(1.0).

The effect of AA6061 thickness on the maximum tensile load and failure mode of CFRP/AA6061 joints was well understood by the fracture processes of joints in the course of lap-shear tensile testing. Besides, the impact of stack-up sequence on failure mode and the maximum tensile load of FDR joints was also discussed in this section. For the FDR joints fabricated with AA6061(1.0) and CFRP, no matter the AA6061(1.0) was placed as the upper or lower workpiece, AA6061(1.0) was the relatively weaker workpiece and torn out in lap-shear tensile testing. Hence, the stack-up sequence has no obvious effect on the failure mode and the maximum tensile load of the FDR joints from AA6061(1.0) and CFRP, which further supports the conclusion that the maximum tensile load and failure mode of a FDR joint are strongly related. Nevertheless, the stack-up sequence exhibited a significant effect on the maximum tensile load and failure mode of

Fig. 12 Fracture process of CFRP/AA6061(2.0) joint. **a** A typical load-displacement curve. **b–e** Deformation modes at different moments, and the corresponding displacements of the joint are marked in **a**



FDR joints from AA6061(2.0) and CFRP. It was found that the failure mode and the maximum tensile load of AA6061(2.0)/CFRP joint differed from those of the CFRP/AA6061(2.0) joint, although the upper or lower CFRP was the failed workpiece and the relatively weaker one compared to AA6061(2.0) in lap-shear tensile testing, which is considered resulting from the following aspects. During lap-shear tensile testing, the shank fold slipped out from the lower CFRP of the AA6061(2.0)/CFRP joint, while the shank head tore the upper CFRP of the CFRP/AA6061(2.0) joint. Note that the diameter of the shank fold (~10.0 mm) is smaller than the shank head diameter (13.5 mm). It is considered that the larger shank head had a stronger locking effect to the CFRP compared to the smaller shank fold, which can be supported by the fact that the maximum inclination angle of blind rivet (i.e., ~40°) on the AA6061(2.0)/CFRP joint was larger than that (i.e., ~25°) on the CFRP/AA6061(2.0) joint reached in lap-shear tensile testing. Therefore, the rivet hole on the lower CFRP was more expanded and there was a larger force component along the rivet axis on the AA6061(2.0)/CFRP joint for a given tensile load, which further increased the chance of the smaller shank fold to slip out from the lower CFRP. Nevertheless, the shank head was too large to slip out from the rivet hole on the upper CFRP of the CFRP/AA6061(2.0) joint and only tore the upper CFRP to fracture, which resulted in a larger maximum tensile load as observed in Fig. 6c.

4 Conclusions

The novel FDR process was successfully applied to joining dissimilar materials (i.e., CFRP and AA6061). The fracture processes of FDR joints were analyzed to understand the effects of AA6061 thickness and stack-up sequence on the mechanical performance of joints in this study. Some conclusions can be drawn as follows:

1. The failure mode and the maximum tensile load of FDR joints are functions of the workpiece thickness and the stack-up sequence, and the maximum tensile load of a FDR joint is strongly correlated with its failure mode.
2. The failure mode and maximum tensile load of FDR joints depend on the relatively weaker one between the upper and lower workpieces, which is the 1.0-mm-thick AA6061 or the CFRP (when AA6061 is thicker than 1.0 mm) disregarding the stack-up sequence.
3. The stack-up sequence does not have an obvious effect on the failure mode and the maximum tensile load of FDR joints from 2.0-mm-thick CFRP and 1.0-mm-thick

AA6061; however, the situation changes when the thickness of AA6061 is larger than 1.0 mm, due to the different locking effects of the shank fold (10 mm in diameter) and shank head (13.5 mm in diameter) on the lower and upper CFRP, respectively.

Funding information This study was funded by the National Natural Science Foundation of China (grant number 51805375) and State Key Laboratory of Mechanical System and Vibration (grant number MSV201814).

References

1. Chung HJ, Rhee KY, Lee B, Lee JH (2009) Effect of oxygen plasma treatment on the bonding strength of CFRP/aluminum foam composite. *J Alloys Compd* 481(1–2):214–219
2. Witik RA, Payet J, Michaud V, Ludwig C, Manson JE (2011) Assessing the life cycle costs and environmental performance of lightweight materials in automobile applications. *Compos A: Appl Sci Manuf* 42(11):1694–1709
3. Barnes TA, Pashby IR (2000) Joining techniques for aluminium spaceframes used in automobiles: Part I-solid and liquid phase welding. *Compos A: Appl Sci Manuf* 99(1–3):62–71
4. Wang H, Yang K, Liu L (2018) The analysis of welding and riveting hybrid bonding joint of aluminum alloy and polyether-etherketone composites. *J Manuf Process* 36:301–308
5. Rodrigues CF, Blaga LA, dos Santos JF, Canto LB, Hage E Jr, Amancio-Filho ST (2014) FricRiveting of aluminum 2024-T351 and polycarbonate: temperature evolution, microstructure and mechanical performance. *J Mater Process Technol* 214(10):2029–2039
6. Fratini L, Ruisi VF (2009) Self-piercing riveting for aluminium alloys-composites hybrid joints. *Int J Adv Manuf Technol* 43(1–2):61–66
7. Lee CJ, Kim JY, Lee SK, Ko DC, Kim BM (2010) Parametric study on mechanical clinching process for joining aluminum alloy and high-strength steel sheets. *J Mech Sci Technol* 24(1):123–126
8. Podlesak F, Hälsig A, Höfer K, Kaboli R, Mayr P (2015) Spin-blind-riveting: secure joining of plastic with metal. *Weld World* 59(6):927–932
9. Gao D, Ersoy U, Stevenson R, Wang PC (2009) A new one-sided joining process for aluminum alloys: friction stir blind riveting. *J Manuf Sci Eng* 131(6):061002
10. Sønstabø JK, Holmstrøm PH, Morin D, Langseth M (2014) Behaviour of flow-drilling screw connections. *Mater Sci Forum* 794-796:413–415
11. Li DZ, Li H, Thornton M, Shergold M, Williams G (2014) The influence of fatigue on the stiffness and remaining static strength of self-piercing riveted aluminium joints. *Mater Des* 54:301–314
12. Wagner J, Wilhelm M, Baier H, Füssel U, Richter T (2014) Experimental analysis of damage propagation in riveted CFRP-steel structures by thermal loads. *Int J Adv Manuf Technol* 75(5–8):1103–1113
13. Cai W, Wang PC, Yang W (2005) Assembly dimensional prediction for self-piercing riveted aluminum panels. *Int J Mach Tools Manuf* 45(6):695–704
14. Sun X, Stephens EV, Khaleel MA (2007) Fatigue behaviors of self-piercing rivets joining similar and dissimilar sheet metals. *Int J Fatigue* 29(2):370–386
15. Krause AR, Chernenkoff RA (1995) A comparative study of the fatigue behavior of spot welded and mechanically fastened aluminum joints. SAE Technical Paper No. 950710

16. Min JY, Li Y, Carlson BE, Jack Hu S, Li JJ, Lin JP (2015) A new single-sided blind riveting method for joining dissimilar materials. *CIRP Ann* 64(1):13–16
17. Szlosarek R, Karall T, Enzinger N, Hahne C, Meyer N (2013) Mechanical testing of flow drill screw joints between fibre-reinforced plastics and metals. *Mater Test* 55(10):737–742
18. Lathabai S, Tyagi V, Ritchie D, Kearney T, Finnin B, Christian S, Sansome A, White W (2011) Friction stir blind riveting: a novel joining process for automotive light alloys. *SAE Int J Mater Manuf* 4(1):589–601
19. Nagel P, Meschut G (2017) Flow drill screwing of fibre-reinforced plastic-metal composites without a pilot hole. *Weld World* 61(5): 1057–1067
20. Wang PC, Stevenson R (2011) Friction stir rivet method of joining: U.S. patent 7862271, pp 1–4
21. Min JY, Li YQ, Li JJ, Carlson BE, Lin JP (2015) Friction stir blind riveting of carbon fiber-reinforced polymer composite and aluminum alloy sheets. *Int J Adv Manuf Technol* 76(5–8):1403–1410
22. Min JY, Li JJ, Carlson BE, Li YQ, Quinn JF, Lin JP, Wang WM (2015) Friction stir blind riveting for joining dissimilar cast mg AM60 and al alloy sheets. *J Manuf Sci Eng* 137(5):051022
23. Ma YW, Li YB, Carlson BE, Lin ZQ (2018) Effect of process parameters on joint formation and mechanical performance in friction stir blind riveting of aluminum alloys. *J Manuf Sci Eng* 140(6): 061007

Publisher's note Springer Nature remains neutral with regard to jurisdictional claims in published maps and institutional affiliations.